Shot Noise and Statistical Parameters for the Estimation of Corrosion Mechanisms.

J.M. Sanchez-Amaya[1], R.A. Cottis[2] and F.J. Botana[1].

[1] Departamento de Ciencia de los Materiales e Ingeniería Metalúrgica y Química Inorgánica. C.A.S.E.M. Universidad de Cádiz. Avda. República Saharaui s/n, Apdo 40, Pto Real, E-11510 Cádiz, Spain

[2] Corrosion and Protection Centre, School of Materials, University of Manchester, P.O. Box 88, Sackville Street, Manchester M60 1QD, United Kingdom (*corresponding author tel 0161 306 4843, fax 0161 306 4865, email bob.cottis@manchester.ac.uk*)

Abstract

In this paper, electrochemical noise measurements on Aluminium AA2014 are reported. Samples were exposed to a range of solutions to promote different corrosion rates and mechanisms. Subsequently, statistical parameters (electrochemical noise resistance, coefficient of variation of current and localization index) and parameters derived from shot noise theory (the low frequency limit of the amplitude of the noise impedance, $Z_{n,f\rightarrow 0}$, the average charge in each event, q, and the frequency of events, f_n) were obtained and related with the type and rate of corrosion. Finally, pairs of shot noise parameters were represented in maps to relate their values with the corresponding corrosion rates and mechanisms.

Keywords: alkaline corrosion, pitting corrosion, electrochemical noise, aluminium, inhibition, passivity

1. Introduction.

Shot noise theory is based in the assumption that the signals are composed of packets of data departing from a base line. This theory can be applied to the analysis of electrochemical noise data from corrosion systems, the current noise signals being considered as packets of charge. Some restrictions to the noise generation processes are necessary when this theory is used in the analysis of electrochemical noise signals [1-4]:

- The current is generated by pulses of the same charge and shape, although both positive-going and negative-going pulses may occur (this is not a necessary condition for the application of the theory to predict noise characteristics from reaction characteristics, although it simplifies the analysis; it is required in order to invert the analysis to compute electrode properties from measured potential and current noise).
- These pulses are statistically independent (this is a necessary condition for the analysis).
- The cathodic reaction is considered to be noiseless, so only the anodic reactions are treated as noise source (this is not a necessary condition, but simplifies the analysis, and is necessary to invert the analysis).
- The two working electrodes have equal corrosion rate (this is not a necessary condition, but simplifies the analysis, and is necessary to invert the analysis).

- The solution resistance is assumed to be zero (this is not a necessary condition for the calculation of the expected behaviour, but it is necessary to invert the analysis).

With these assumptions, we can obtain from the voltage and current noise signals the charge in each event, q, and the frequency of appearance of these events, f_n [1-5]:

$$q = \frac{\sqrt{\psi_E}\sqrt{\psi_I}}{B} \quad (1)$$

$$f_n = \frac{B^2}{\psi_E A} \quad (2)$$

where ψ_E and ψ_I are the low frequency PSD values of the potential and current noise, respectively, B is the Stern-Geary coefficient and A the electrode area exposed. Note that in earlier work f_n has been described as the frequency over the specimen, so the A term has been omitted. The representation as a frequency per unit area appears more logical, and has therefore been adopted in this paper.

In order to accommodate systems where the required assumptions may not be strictly valid, the term 'characteristic charge' has been proposed for q and 'characteristic frequency' for f_n [1].

These two parameters derived from shot noise theory have been reported to provide information related to the nature of the corrosion processes [1-4]. Thus, q gives an indication of the mass of metal lost in the event, while f_n provides information about the

rate at which these events are happening [5]. Therefore, a system undergoing active uniform corrosion can have both large charge and frequency. Localized corrosion, such as pitting, can be characterized by a small number of events, and is therefore expected to have a low frequency and high charge. Finally, in the case of passivity, the charge is expected to be low, while the frequency will depend on the processes occurring on the passive film [5].

The noise impedance (strictly the amplitude of the noise impedance, since it is not possible to extract phase information) can also be derived from ψ_E and ψ_I according to equation 3:

$$Z_n = \sqrt{\frac{\psi_E}{\psi_I}} \tag{3}$$

and $Z_{n,f\to 0}$, the limit of Z_n as the frequency tends to zero, is expected to be comparable with R_p [1]. Since $I_{corr} = B/R_p$, and $I_{corr} = qf_n$, $Z_{n,f\to 0}$ is related to f_n and q according to equation 4:

$$qf_n = B / Z_{n,f\to 0} \tag{4}$$

In the recent literature [6,7] q and f_n have been compared with statistical parameters in order to test their reliability. These statistical parameters were the electrochemical noise resistance (R_n), the coefficient of variation of current (CV) and the localization index (LI), which are defined in the equations 5 to 7, respectively:

$$R_n = \frac{\sigma_E}{\sigma_I} \tag{5}$$

$$CV = \frac{\sigma_I}{\bar{I}} \tag{6}$$

$$LI = \frac{\sigma_I}{rms(I)} = \frac{\sigma_I}{\sqrt{\frac{1}{N}\sum_{k=1}^{N} I_k^2}} \tag{7}$$

where σ_E is the standard deviation of potential; σ_I, the standard deviation of current and $\bar{I}$, the mean current. Although R_n is strictly inversely proportional to the corrosion rate only in the particular case of uniform corrosion under activation control, it is generally accepted that high R_n values are associated to low activity [3]. *CV* and *LI* have been experimentally related to corrosion mechanism, with large values of *CV* and/or *LI* suggested as indicators of localized corrosion, although these parameters have serious theoretical limitations [5, 8].

More recently, the Pitting Factor (PF) has been proposed by Eden [9]. This is defined as the standard deviation of current divided by the corrosion current (or the corrosion current density times the specimen area). Other than problems with the expected dependence of PF on specimen area, and on the assumption that R_n is equivalent to R_p, this parameter is expected to correlate with f_n, [6] and it is not therefore considered further here.

Shot noise theory has been recently applied to the study of different types of corrosion [6, 7]. The behaviour of carbon steel immersed in different solutions was studied using electrochemical noise measurements. The solutions employed were intended to provoke different corrosion mechanisms, such as pitting, inhibition and uniform corrosion. This allowed the construction of corrosion maps, where the position in a map can be related with the activity or the type of corrosion. However, these maps have been developed only for carbon steel. In this paper, therefore, shot noise theory has been applied to the analysis of electrochemical noise signals of aluminium alloy AA2014 in a range of solutions. The metal-environment systems employed here produced a range of different corrosion types and activities, and the corrosion behaviour has been correlated with the values of the various parameters.

2. Experimental.

Material.

A sample of AA2014-T3 sheet was used, the chemical composition of which is given in Table 1.

Specimen Preparation.

The specimen dimensions were 200 x 15 x 1 mm. The samples were immersed in the solutions to a depth of 70 mm, giving an exposed area of 21 cm^2, and allowing the part not immersed to be electrically connected to the electrochemical noise measurement equipment. In cases when it was necessary (notably in pitting corrosion) the non-exposed zones of samples were covered with "Lacomit number 65441" lacquer in order to avoid preferential attack at the water line. The samples were chemically cleaned,

initially in 2.5 M NaOH for 2 minutes, then in 15% HNO_3 for 15 seconds (in order to eliminate the corrosion products formed in the first step). Finally, the specimens were rinsed with deionised water and dried with laboratory paper before testing.

Environment.

The test solutions used are listed in Table 2.

Test Methods.

Visual examination of the specimens was carried out after the experiments to check that they suffered the expected type of corrosion. Three samples were tested in each solution, in order to verify the reproducibility of the results.

Electrochemical noise time records were obtained using a Gill AC instrument (ACM Instruments) controlled by means of the Sequencer program. This program was used in Current & Voltage / time mode, in order to measure the current and the potential simultaneously. A saturated calomel electrode (SCE) was used as reference electrode for potential measurement. The measurement rate registered was one point per second. In order to reduce aliasing problems, the Antialiasing option was activated in the software, so each point registered in the records was the mean value of 30 consecutive readings. This provides a form of low-pass filtering that will reduce the amplitude of frequencies in the range 0.5 to 15 Hz. Each test consisted of 10 consecutive measurements, each composed of 1024 points. Before each record, 2576 seconds had lapsed; so one record per hour was measured, obtaining 10 records per test.

A value of B of 0.026 V per decade has been assumed in the analysis. This result is obtained for common values of the Tafel slopes for the anodic and cathodic reactions. Variations in this value will not affect the relative behaviour of the various systems, unless there is a significant difference between the true B values for the various environments.

Data analysis.

In most Figures presented in the present paper, the cumulative probability, p, has been plotted as a function of the various parameters (R_n, LI etc.). In order to obtain the cumulative probability the parameter values were sorted into ascending order and p derived as $n/(N+1)$, where n is the position of the value in the sorted list, and N is the total number of values (1024 for these experiments). This way of showing the results has been used previously [6] and allows one to see clearly the distribution of the values. Hence, the plotted values in this representation can be easily compared. In addition, another kind of representation has been used in this paper, consisting of plotting one parameter against another, allowing one to build corrosion maps of rates and mechanisms [7]. In this case the density of the points gives a visual indication of the probability.

3. Results and Discussion.

From the visual examination it was observed that the AA2014 undergoes the expected corrosion mechanism for each solution, that is pitting corrosion in NaCl, uniform

corrosion in NaOH and inhibition/passivation in NaCl+$Ce(NO_3)_3$ and $Ce(NO_3)_3$ [11-14].

Figures 1 and 2 show examples of potential and current records corresponding to AA2014 in the indicated solution after 3 hours of immersion. It can be seen in Figure 1 that the activity of each solution is reflected in the mean potential values. Thus, AA2014 in NaOH 0.01M gives the lowest free corrosion potential of the systems plotted in this figure (about –1090 mV vs. SCE), indicating the high activity of this system. The most positive potential is observed in 0.03 M $Ce(NO_3)_3$, confirming the passivity of this alloy in Ce-containing solutions. Figure 2 shows the current signals corresponding to the potential records in Figure 1. If the amplitude of the fluctuations of Figure 2 is taken as a first approximation of the activity, similar conclusions to the ones obtained from Figure 1 are reached. So, the AA 2014 corrodes more actively in NaOH 0.01M, while it shows low activity in the presence of Ce^{3+} ions.

Statistical Analysis.

The first statistical parameter studied here was the electrochemical noise resistance (R_n). Before calculating this parameter, the drift was removed from both current and potential records by means of a linear regression subtraction, commonly recommended in the literature for the calculation of statistical parameters [1, 3, 15-17]. In Figure 3, the R_n values as a function of the indicated solution have been included (the correspondence between the codes and the electrolytes can be seen in Table 2). Figure 3 shows that R_n can distinguish between the different corrosion activities of AA2014 in the media tested. So, the more aggressive medium is NaOH (except 10^{-3} M, because the

concentration is very low), followed by NaCl and NaCl + $Ce(NO_3)_3$, with $Ce(NO_3)_3$ being least aggressive.

Next, the results of the estimation of the coefficient of variation of current (CV) and localization index (LI) are presented. These statistical parameters are defined above and have been related to the corrosion mechanism [5, 8], with a value of 1 or more (or approaching 1 in the case of LI, which is limited to an upper bound of 1) being taken as indicative of localized corrosion.

Figures 4 and 5 present the CV and LI values obtained. It can be seen that the probability curves for these parameters for the different media overlap. In addition, it can be seen that the highest values were obtained when NaOH media was used, which does not follow the expected tendency, since AA2014 in NaOH undergoes uniform corrosion. This was probably a result of the effect of hydrogen bubble generation (this is discussed further below). These observations support the view that these parameters are unreliable as indicators of localized corrosion.

Shot Noise Parameters.

The shot noise theory presented above is based on the assumption that the power spectrum associated with an individual transient will be constant at low frequencies (where low implies frequencies with a period that is longer than the duration of individual transients, and where many transients occur within one period of the analysis frequency). Thus the ideal analysis will use the PSDs determined at the lowest possible frequency in order to estimate q and f_n, and the PSD should take the form of a low frequency plateau. However, in many cases, PSD changes with frequency over the

whole range, that is, no low frequency plateau is seen (it should be noted that this can also occur if an inappropriate order is used to determine the MEM). In these cases, the best option is probably to take the PSD value corresponding to the lowest frequency [2,5], and in this work the PSD values at 10^{-3} Hz (the minimum frequency available) were taken to estimate q, f_n and $Z_{n,f\to 0}$.

As the first stage of the analysis, linear trend removal was used to compensate for non-stationary components of the signals. The PSD was calculated by means of both the Fast Fourier Transform (FFT) and the Maximum Entropy Method (MEM), so that q and f_n values obtained with the two techniques can be compared. In Figure 6 the influence of the order used in the determination of the MEM is plotted. It can be seen that when high orders are used (300), the power spectrum shows large fluctuations at high frequencies, and generally appears similar to the power spectrum obtained using the FFT. In contrast, the use of low orders implies loss of information since the correlation with the spectrum obtained by FFT is poor, notably at low frequencies. For this work an order of 50 was used, being high enough to avoid poor correlation with the FFT spectra, and at the same time producing reasonably smooth spectra and hence averaging the low frequency PSD effectively.

In Figures 7 to 10, the values of the shot noise parameters, q and f_n have been plotted. It can be seen that most q values obtained lie in the range 10^{-9} to 10^{-4} C, while most f_n values were between 10^{-2} and 10^{3} Hz/cm^2.

In Figures 7 and 8, the q values using FFT and MEM respectively, have been included. If the q values of Figures 7 and 8 are compared, very little difference can be found

between the use of FFT and MEM, that is, both methods lead to similar results. From the point of view of the shot noise analysis, the higher the value of q, the more charge in each event, that is, the more mass is being lost in each anodic event [5]. In Figures 7 and 8 it can be seen that the highest values of q are reached in NaOH, although the values depend on the concentration. So, the order of q values is A>B>D>C.

The values of f_n obtained by means of FFT and MEM are presented in Figures 9 and 10, respectively. No significant differences between the f_n values using FFT and MEM were found. This parameter estimates the frequency of events [5]. In Figures 9 and 10 it is not possible to distinguish between the different systems (A≅B≅C≅D). However, these figures do differentiate between the concentrations of NaOH. So, the higher concentrations of NaOH produce the higher values of f_n. Note that R_n also was able to distinguish between different concentrations of NaOH.

It seems probable that the EN for the NaOH solutions will be dominated by hydrogen bubble nucleation, growth and separation, which has been studied by Gabrielli et al. [18]. This has some of the character of a shot noise process, although some of the required assumptions are not applicable. However, it seems reasonable to expect that f_n will correlate with bubble emission frequency and q with the amplitude of the fluctuation in current associated with bubble emission. On this basis the results for the NaOH solutions seems reasonable, with slightly increasing values of q for more dilute solutions (implying larger bubbles), but significantly lower values of f_n (implying a much slower rate of bubble emission).

Parameter Maps.

In Figures 11 (with an enlargement of the central region in Figure 12), the values of $Z_{n,f\to 0}$, f_n and q for each time record have been plotted as a map. $Z_{n,f\to 0}$ has been used in this case rather than R_n because this allows all three parameters to be plotted in a single map by virtue of the relationship of equation 4 (while R_n and $Z_{n,f\to 0}$ are not the same for a particular time record, they do exhibit a general equivalence, as is evidenced in the comparison of Figure 12). Since the FFT and MEM algorithms lead to similar values, only the values obtained from the MEM have been included here. Figure 11 can be considered as a map of corrosion rate and type, with higher corrosion rates towards the bottom of the map, and lower frequency (hence possibly more localized) processes towards to left. In work on carbon steel [5] it has been found that pitting occupied the left of the diagram at relatively low values of $Z_{n,f\to 0}$, uniform corrosion occupied the lower right of the diagram (low $Z_{n,f\to 0}$ and high f_n), and inhibited or passive systems occupied the top of the diagram (high $Z_{n,f\to 0}$). For the aluminium alloys studied here the behaviour is slightly different. In particular, uniform corrosion in concentrated NaOH solution occupied a similar position to that for carbon steels, but more dilute solutions move up and to the left into the region where localized corrosion is found for carbon steels. This is probably because of the dominant role of hydrogen bubble emission, rather than the anodic process, on noise generation in these systems. The lower concentration active corrosion data thus overlap the data for localised corrosion. As with carbon steels the inhibited and passive systems are characterized primarily by a high value of $Z_{n,f\to 0}$, with a rather variable value of f_n.

4. Conclusions.

In this paper, the values of some statistical parameters and other derived from shot noise theory have been calculated for electrochemical noise records of AA2014 immersed in different solutions. NaOH was used to provoke uniform corrosion, NaCl for pitting, $Ce(NO_3)_3$ for passivation, and NaCl+$Ce(NO_3)_3$ for inhibition. Visual examination of the samples after testing confirmed the expected corrosion mechanisms and activities.

Noise resistance (R_n) distinguished between the systems studied. Thus, the R_n values were clearly different when the media were NaOH, NaCl, NaCl+$Ce(NO_3)_3$ and $Ce(NO_3)_3$. In addition, a correlation between the concentration of the media and R_n was found. However, neither the coefficient of variation of current (CV) nor the localization index (LI) could distinguish properly between the different corrosion mechanisms.

The parameters based on the shot noise analysis provided some discrimination of the various corrosion processes, although the discrimination was less clear than was found in previous work on steel. The characteristic charge, q, could discriminate between the corrosion rates and mechanisms quite well. The characteristic frequency, f_n, could differentiate between the different corrosion rates for uniform corrosion, that is, between different concentrations of NaOH, but it did not discriminate between the low concentration active corrosion and pitting corrosion.

A corrosion map has been constructed that represents the q, f_n and $Z_{n,f\to 0}$ values of all of the time records. The regions in which the results for the various forms of corrosion are found differ a little from previous results on carbon steels, but this can be rationalised in terms of the different noise generation process (hydrogen bubble emission rather than active metal dissolution) for the two systems.

While the observations of this work suggest that the relationship between the shot noise parameters and the rate and type of corrosion is not as simple as might be hoped, these parameters do appear to provide relatively intuitive descriptors of the nature of the relevant electrochemical processes. Thus, for active corrosion the q and f_n values seem to relate in a logical way to the anodic hydrogen bubble evolution process, although further work is needed to confirm this.

5. Acknowledgments.

This work has been financed by the European Community (Contract Nº HPMT-CT-2000-00087), the Interministerial Commission for Science and Technology of Spain, project MAT2001-3477 and by the Junta de Andalucía.

6. References.

[1] R.A. Cottis. *Corrosion*, Vol. 57, Nº 3, (2001), pp.265-285.

[2] R.A. Cottis and S. Turgoose, *Materials Science Forum*, Vols. 192-194 (1995) pp. 663-672.

[3] R.A. Cottis and S. Turgoose, "Electrochemical Impedance and Noise". Corrosion Testing Made Easy, NACE International, 1999.

[4] U. Bertocci and F. Huet, *Corrosion*, Vol. 51, No 2, pp 131-144 (1995).

[5] R.A. Cottis, M.A.A. Al-Awadhi, H.A. Al-Mazeedi and S. Turgoose, *Electrochimica Acta*, **46** (2001) pp. 3665-3674

[6] H.A. Al-Mazeedi and R.A. Cottis, *Electrochimica Acta*, 49 (2004) pp. 2787-2793.

[7] H.A. Al-Mazeedi and R.A. Cottis, Corrosion/2004, NACE. New Orleans, Louisiana. Paper 04460 (2004) pp. 1-10.

[8] F. Mansfeld and Z. Sun. *Corrosion.* 55 (1999) pp. 915-918.

[9] D.A. Eden, B. Breen, Corrosion/2003, NACE. San Diego, CA. Paper 03361 (2003).

[10] W. Hufnagel. "*Manual del Aluminio*". Ed. Reverté, 1992. P.1063

[11] M. Bethencourt, F.J. Botana, J.J. Calvino, M. Marcos, M.A. Rodríguez-Chacón. *Corrosion Science*, Vol. 11 (1998) pp. 1803-1819

[12] M.A. Arenas, M. Bethencourt, F.J. Botana, J. Damborenea, M. Marcos. *Corrosion Science,* Vol. 43 (2001) pp. 157-170

[13] A. Aballe, M. Bethencourt, F.J. Botana, M. Marcos. *Journal of Alloys and Compounds* Vol. 323-324 (2001) pp. 855-858

[14] A. Aballe, M. Bethencourt, F.J. Botana, M. Marcos, R. Osuna. *Electrochimica Acta* Vol. 47 (2002) pp. 1415-1422

[15] F. Mansfeld, Z. Sun, C. H. Hsu. *Electrochim. Acta* 46 (2001) 3651-3664.

[16] F. Mansfeld, Z. Sun, C. H. Hsu, A. Nagiub. *Corr. Sci*. 43 (2001) 341-352.

[17] U. Bertocci, F. Huet, R.P. Nogueira, P. Rousseau. *Corrosion* 58 (2002) 337-347.

[18] C. Gabrielli, F. Huet and M.Keddam, *Journal of Applied Electrochemistry* Vol. 15, No. 4, pp. 503-508 1985

Figure Captions

Figure 1. Examples of Potential records corresponding to AA2014 in the indicated media after 3 hours of immersion

Figure 2. Examples of Current records corresponding to AA2014 in the indicated media after 3 hours of immersion

Figure 3. R_n values after removing the first order fitted polynomial.

Figure 4. Values of coefficient of variation of current (*CV*).

Figure 5. Values of localization index (*LI*).

Figure 6. PSD plots estimated by means of FFT and MEM with different orders. A potential record of AA2014 in NaCl after 8 hours has been included in the Figure as example.

Figure 7. Values of q using Fast Fourier Transform (FFT) to estimate PSDs.

Figure 8. Values of q using Maximum Entropy Method (MEM) to estimate PSDs.

Figure 9. Values of f_n using Fast Fourier Transform (FFT) to estimate PSDs.

Figure 10. Values of f_n using Maximum Entropy Method (MEM) to estimate PSDs.

Figure 11 Map of $Z_{n,f\to 0}$, f_n and q for all time records. All values are estimated from the low frequency limit of the MEM spectra.

Figure 12 Comparison between R_n and $Z_{n,f\to 0}$. Each point plotted corresponds to the data for a particular time record, while the solid line corresponds to $R_n = Z_{n,f\to 0}$.

Table 1 Composition (wt %) of aluminium alloy AA2014.

Si	Fe	Cu	Mn	Mg	Zn	Ni	Cr	Pb
0.92	0.51	4.67	0.78	0.64	0.082	0.029	0.017	0.006
Sn	Ti	Ag	B	Zr	V	Ga	P	Al
0.009	0.022	0.001	0.001	0.003	0.002	0.005	0.001	92.294

Table 2. Concentration of solutions used as the electrolyte of AA2014 to achieve the mechanism indicated. The last row includes the code used for each electrolyte.

Dominant Mechanism	Uniform Corrosion				Pitting			Passivation			Inhibition		
Solution	NaOH (M)				NaCl (M)			$Ce(NO_3)_3$ (M)			NaCl 0.6M +$Ce(NO_3)_3$ (M)		
Concentration	0.1	0.05	0.01	0.001	2	0.6	0.1	0.03	0.005	0.001	0.03	0.005	0.001
Code	A1	A2	A3	A4	B1	B2	B3	C1	C2	C3	D1	D2	D3

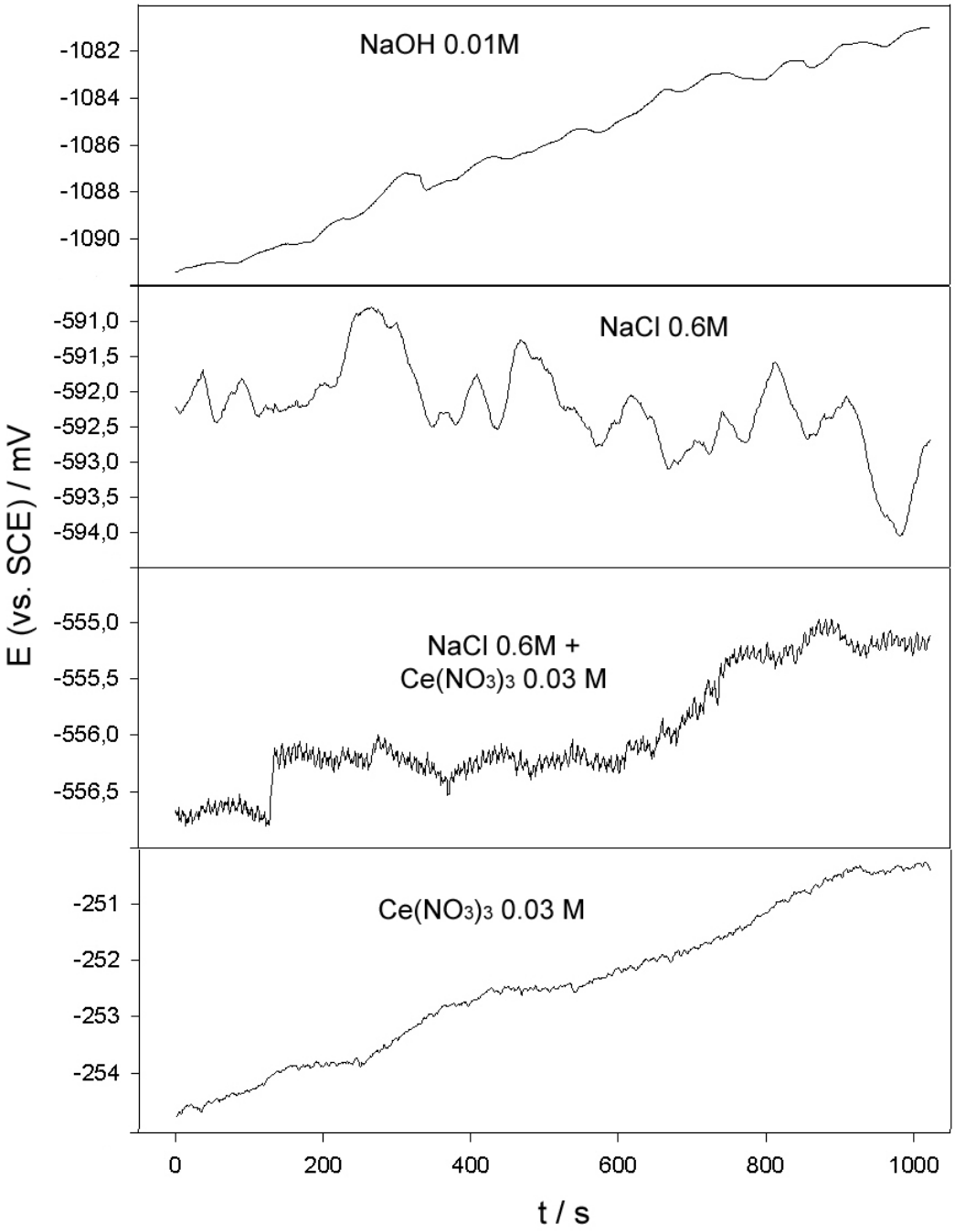

Figure 1. Examples of Potential records corresponding to AA2014 in the indicated media after 3 hours of immersion

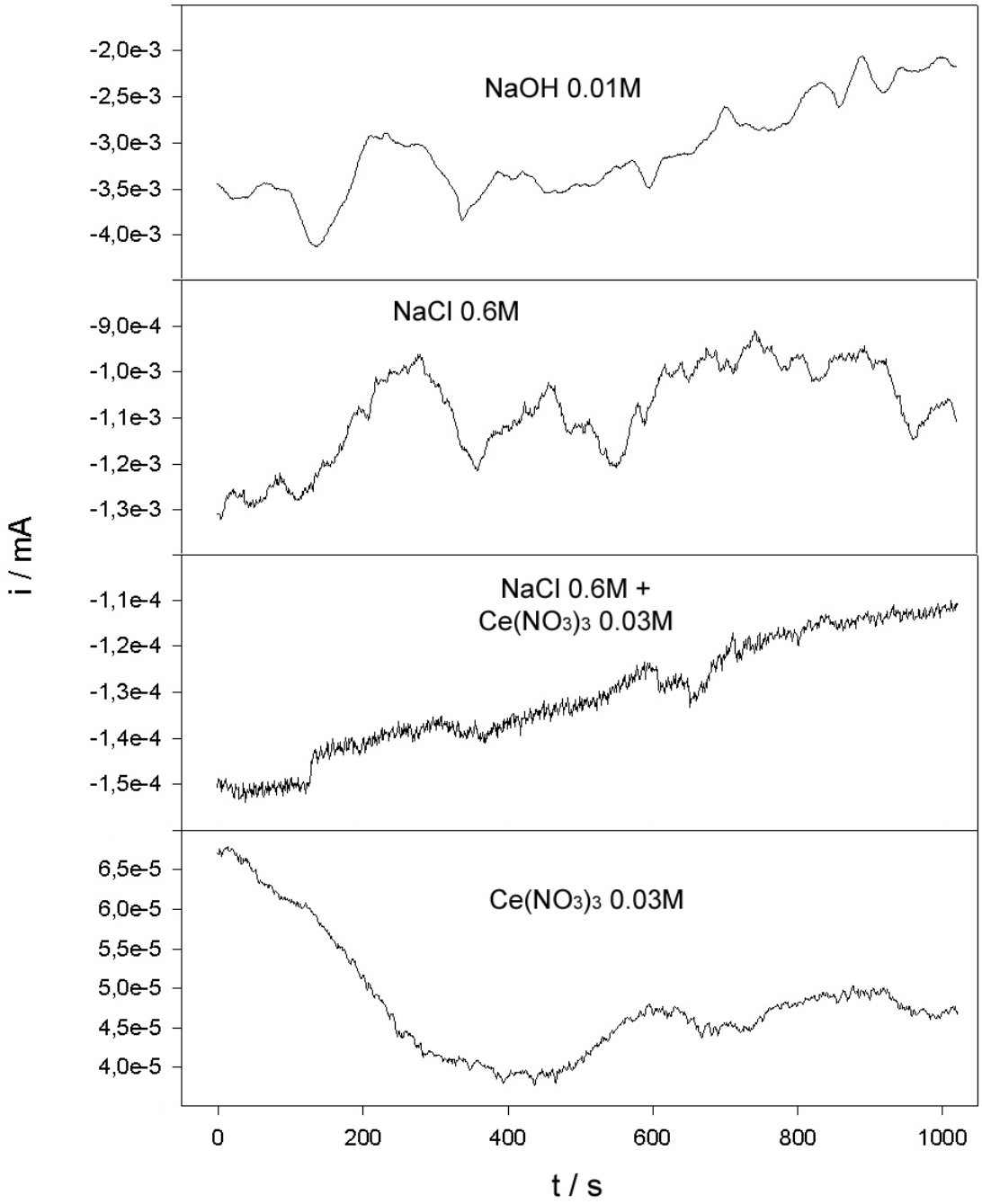

Figure 2. Examples of Current records corresponding to AA2014 in the indicated media after 3 hours of immersion

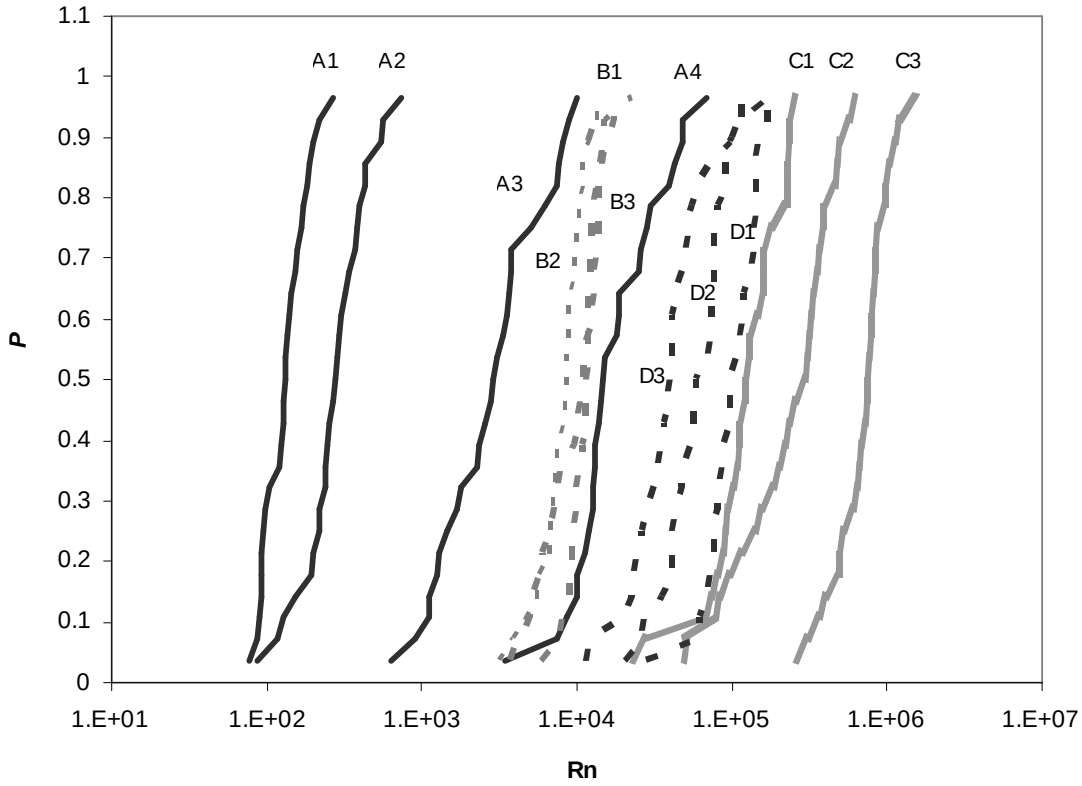

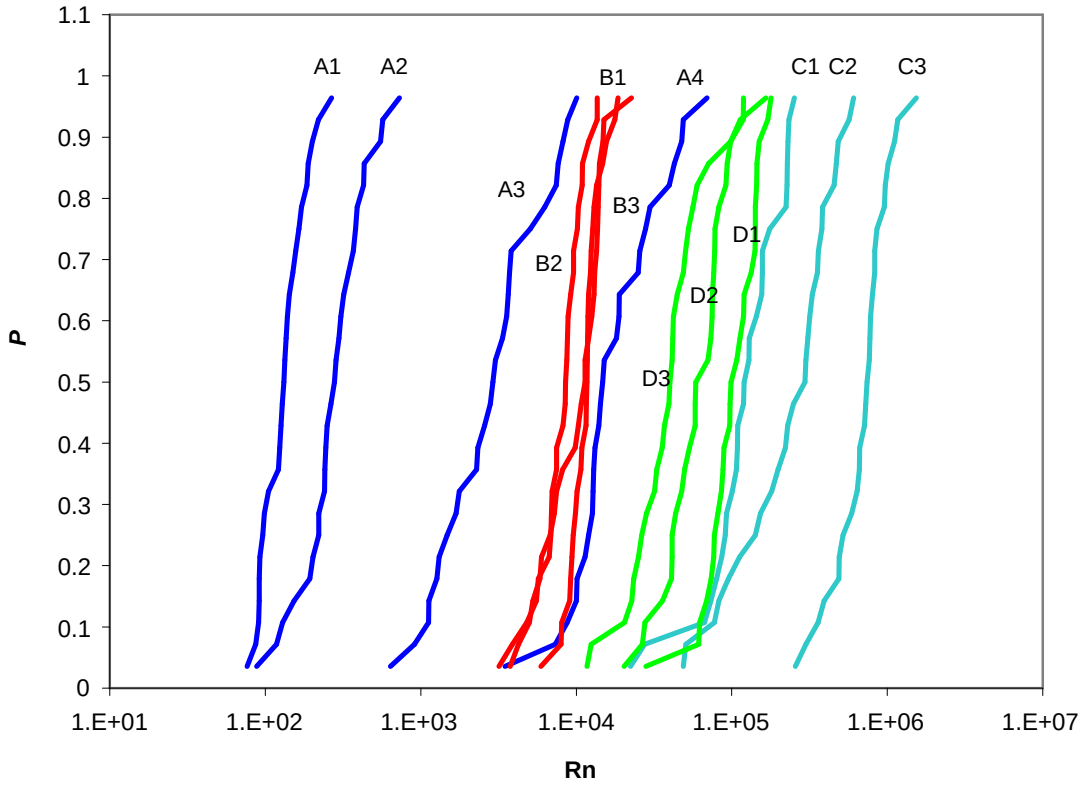

Figure 3. R_n values after removing the first order fitted polynomial.

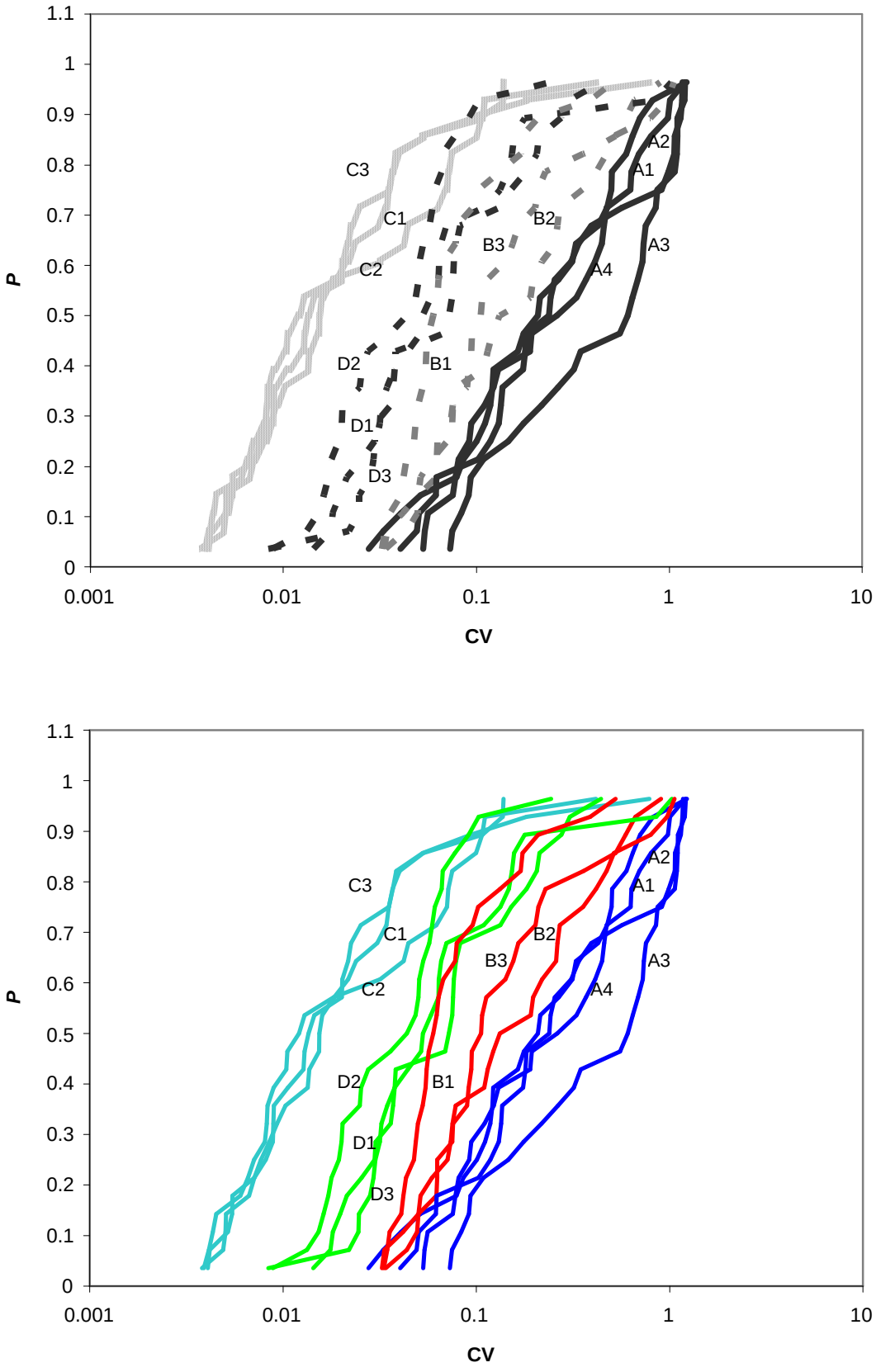

Figure 4. Values of coefficient of variation of current (*CV*).

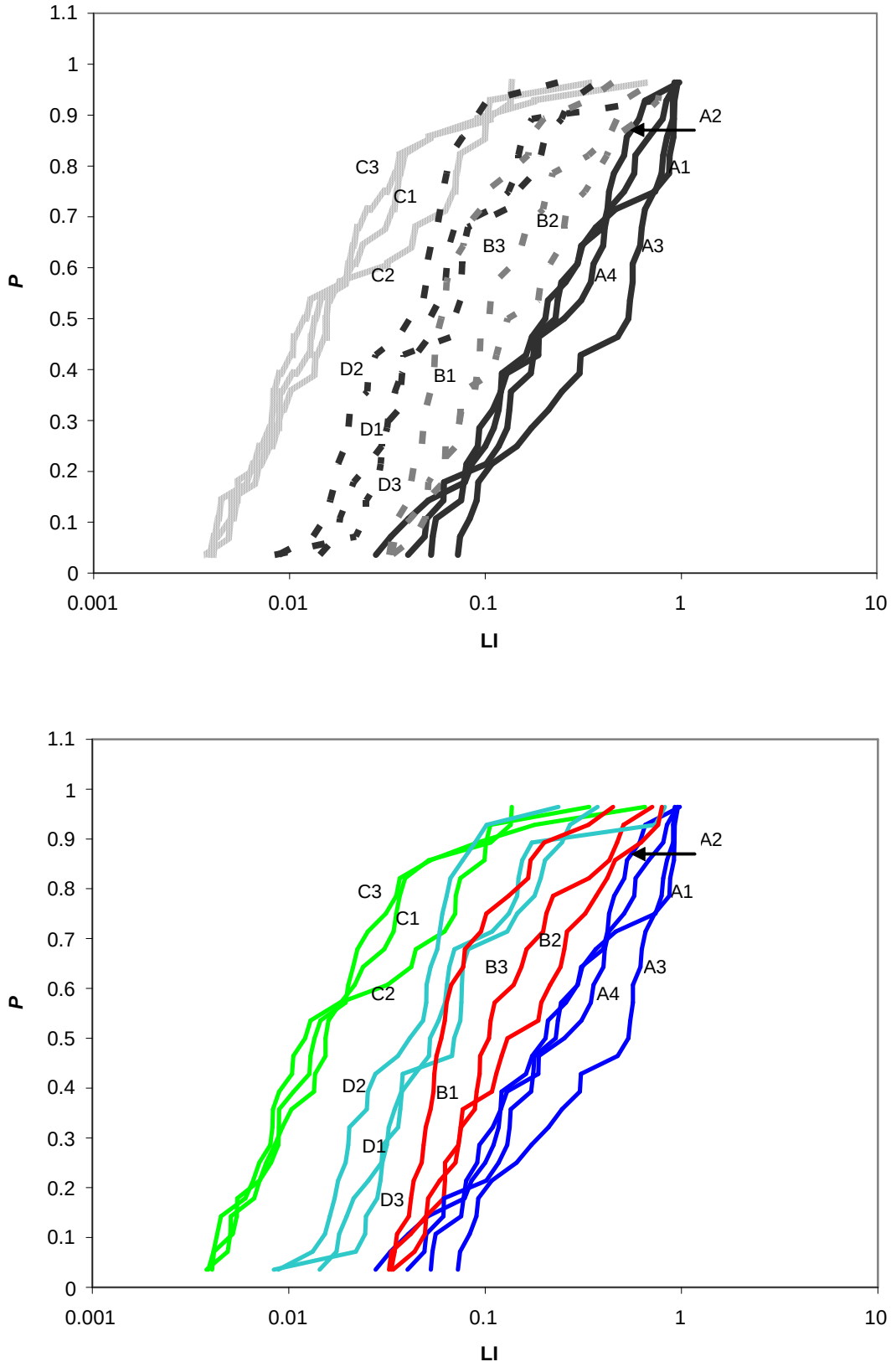

Figure 5. Values of localization index (*LI*).

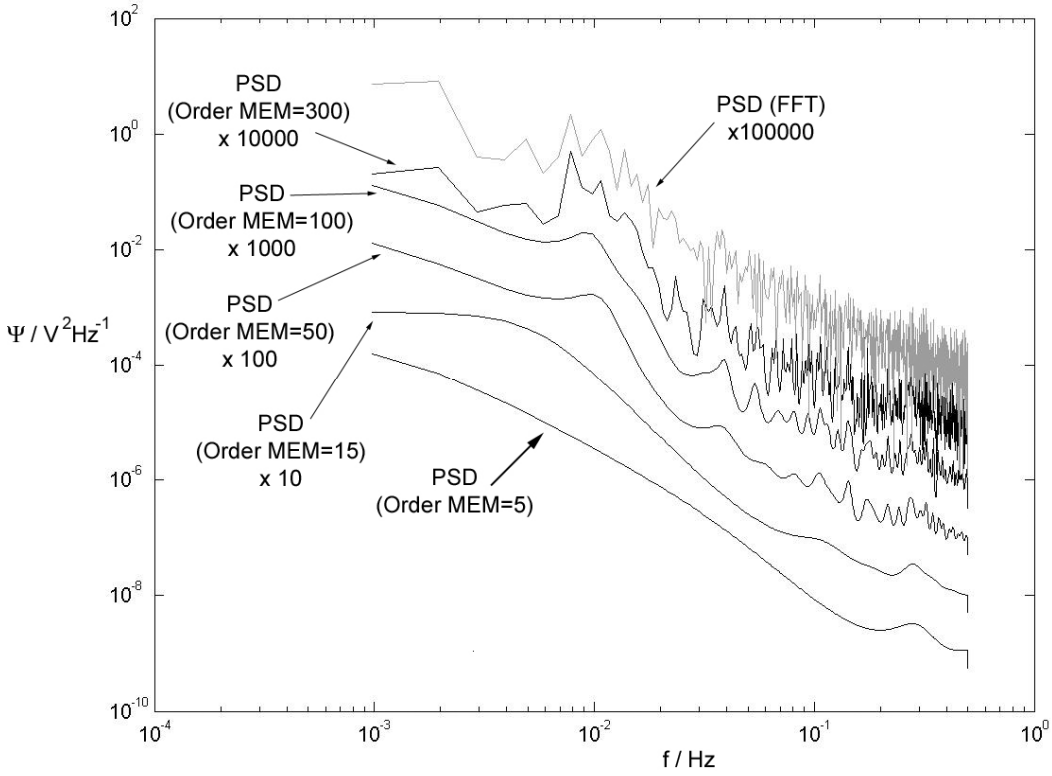

Figure 6. PSD plots estimated by means of FFT and MEM with different orders. A potential record of AA2014 in NaCl after 8 hours has been included in the Figure as example.

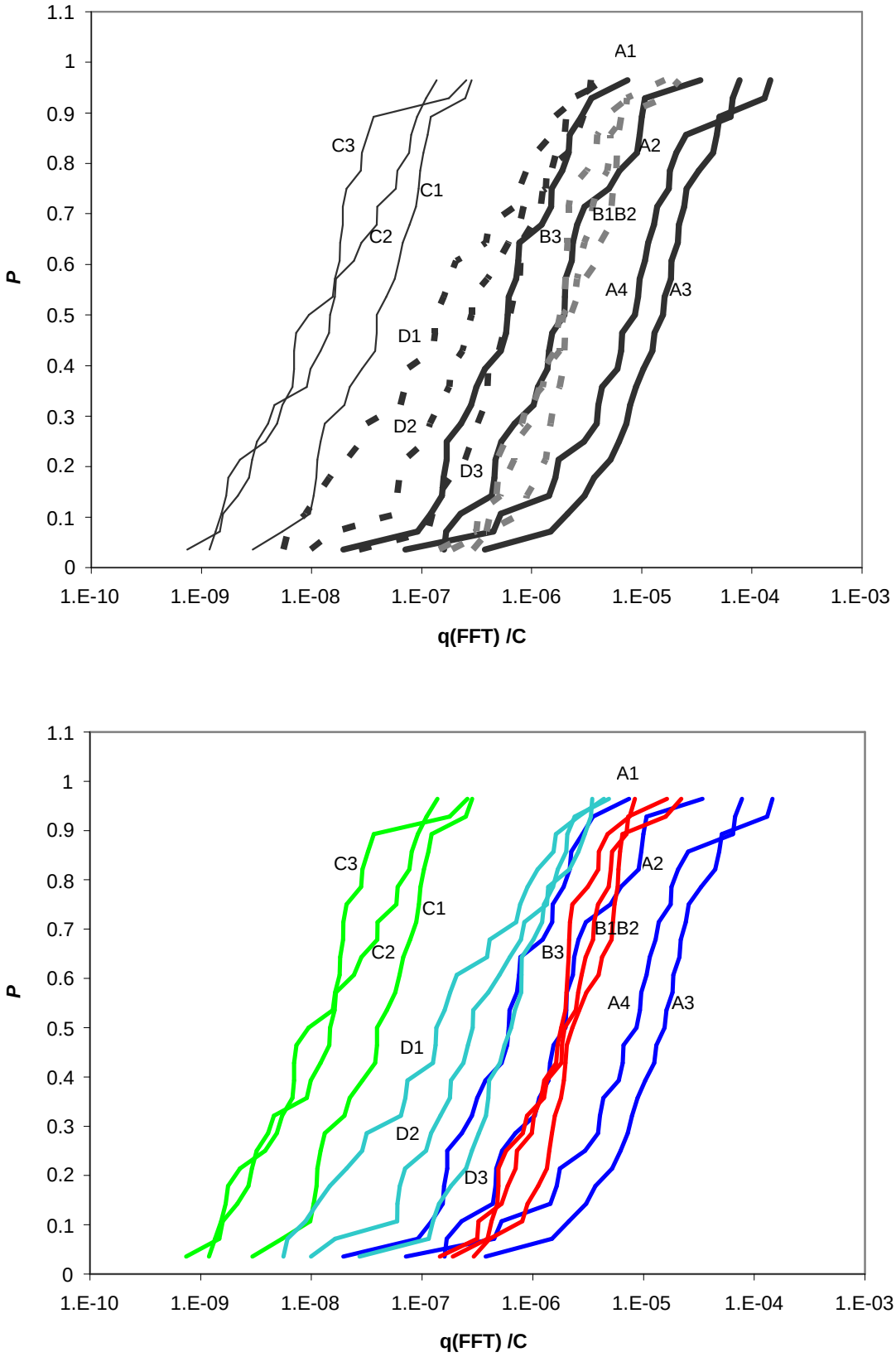

Figure 7. Values of *q* using Fast Fourier Transform (FFT) to estimate PSDs.

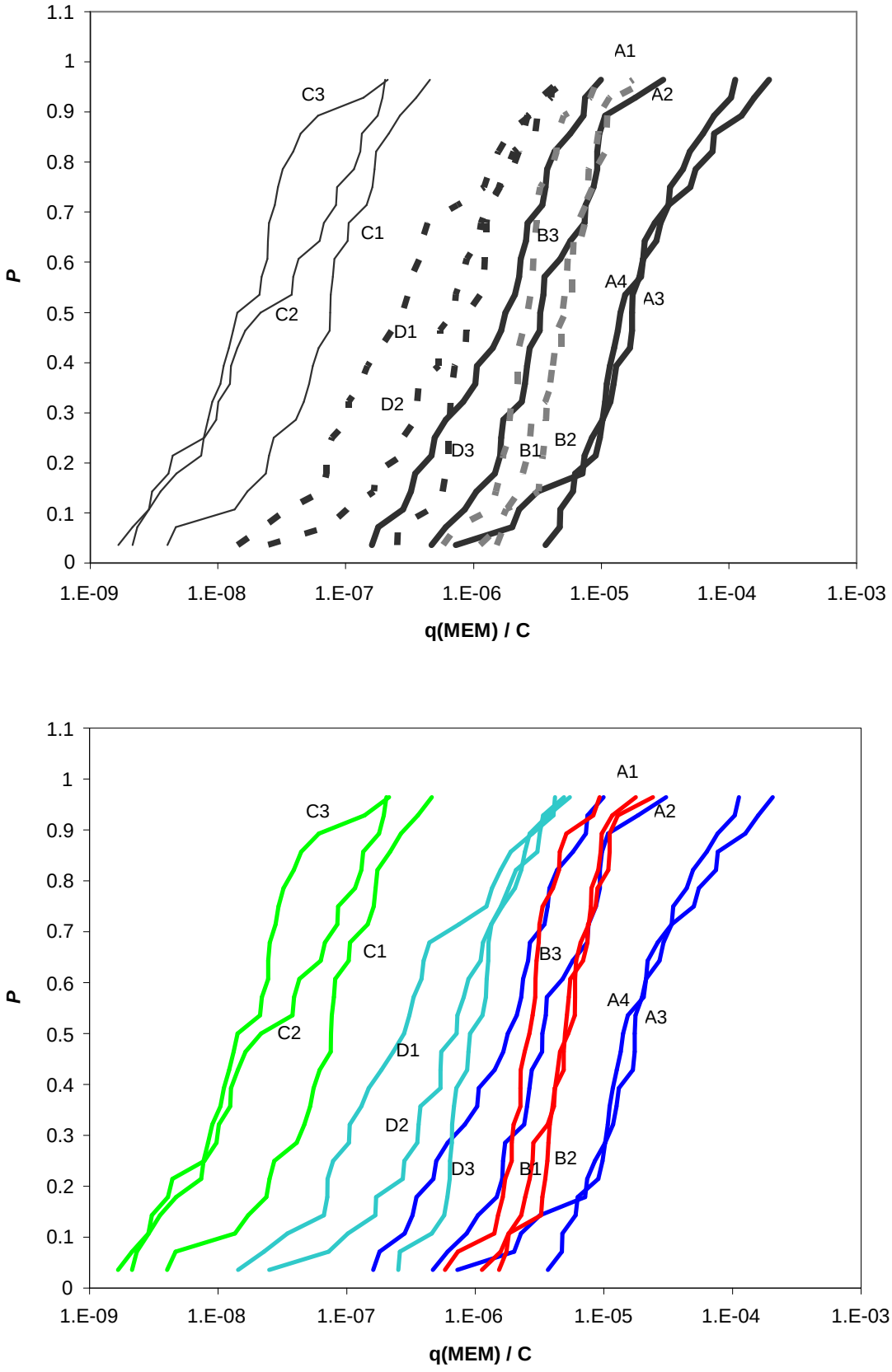

Figure 8. Values of *q* using Maximum Entropy Method (MEM) to estimate PSDs.

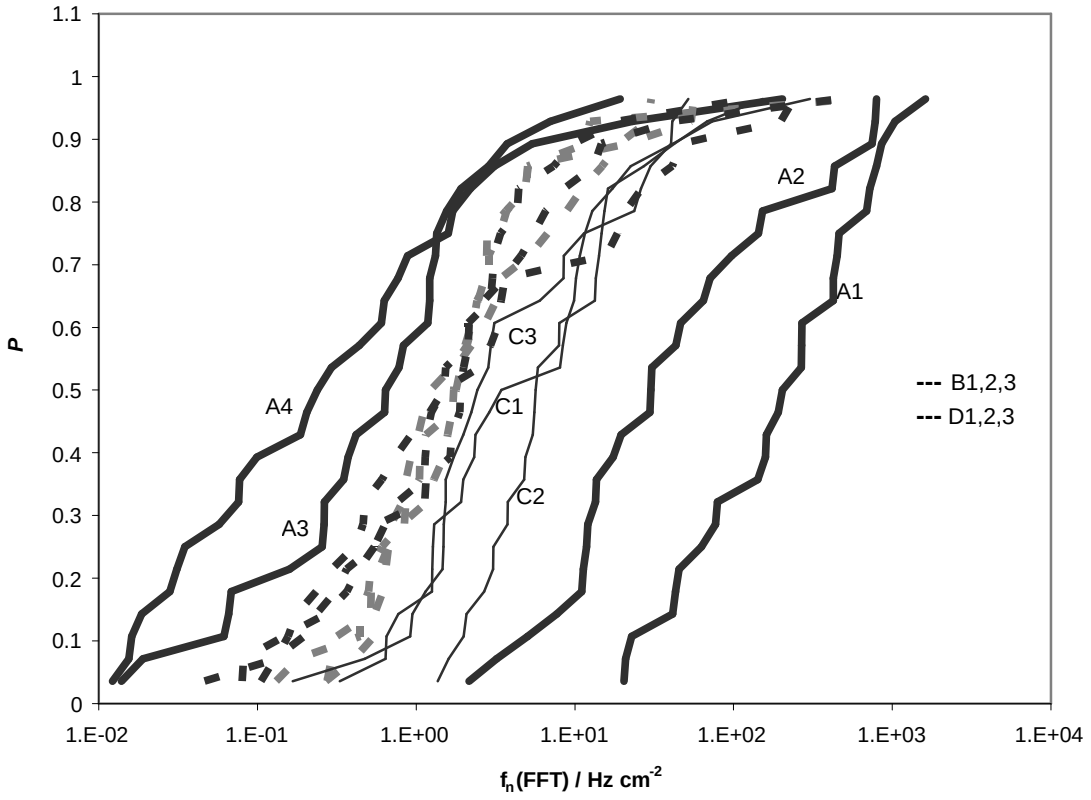

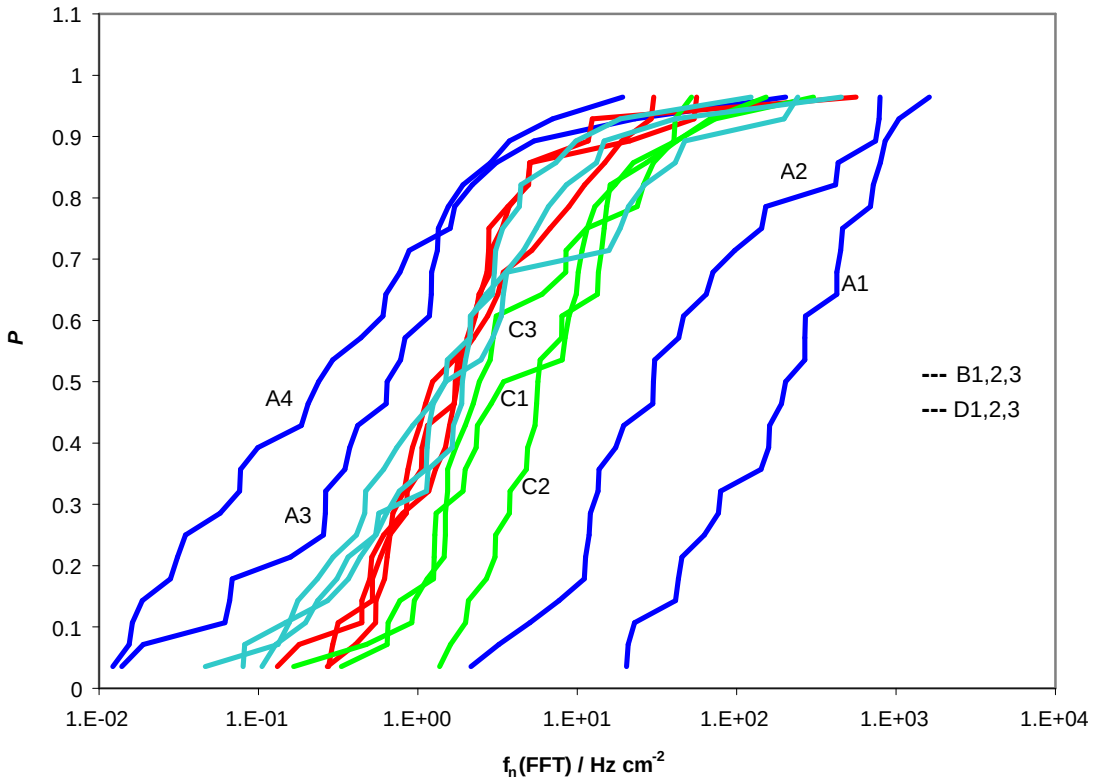

Figure 9. Values of f_n using Fast Fourier Transform (FFT) to estimate PSDs.

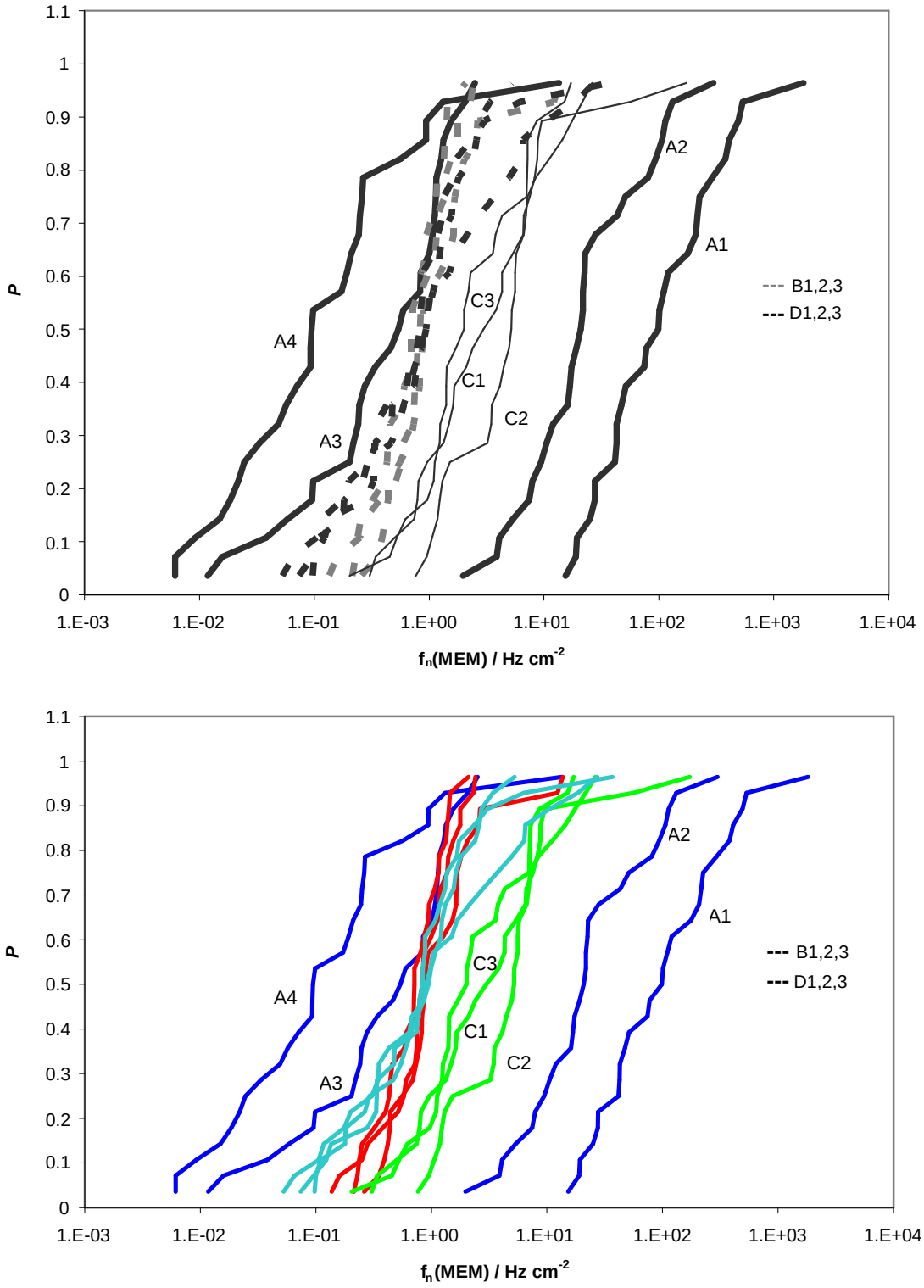

Figure 10. Values of f_n using Maximum Entropy Method (MEM) to estimate PSDs.

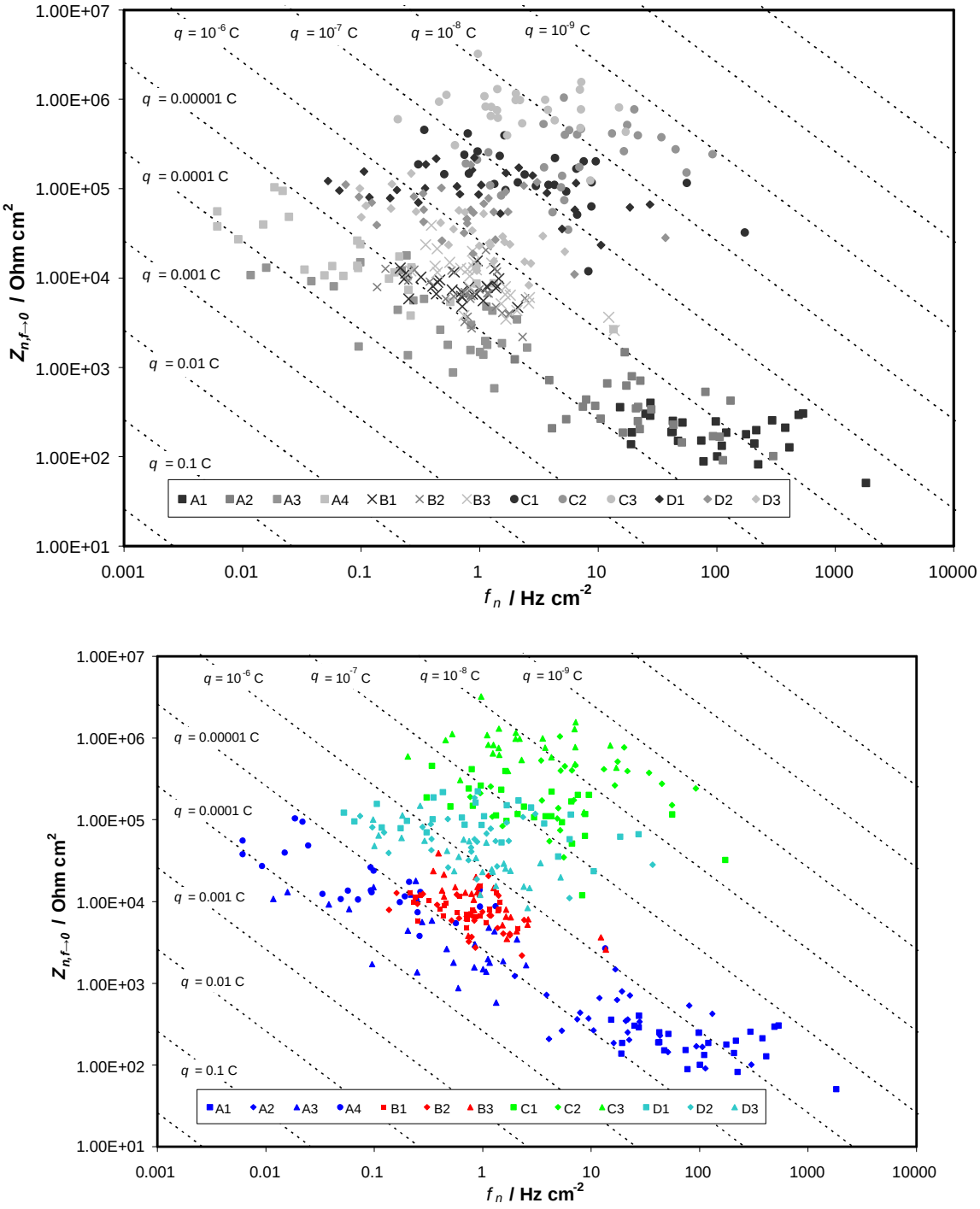

Figure 11 Map of $Z_{n,f\to 0}$, f_n and q for all time records. All values are estimated from the low frequency limit of the MEM spectra. It is difficult to discriminate between the various tests on the printed black and white version of this figure. In the electronic version colour is used to make this clearer, or the figure can be obtained from the authors.

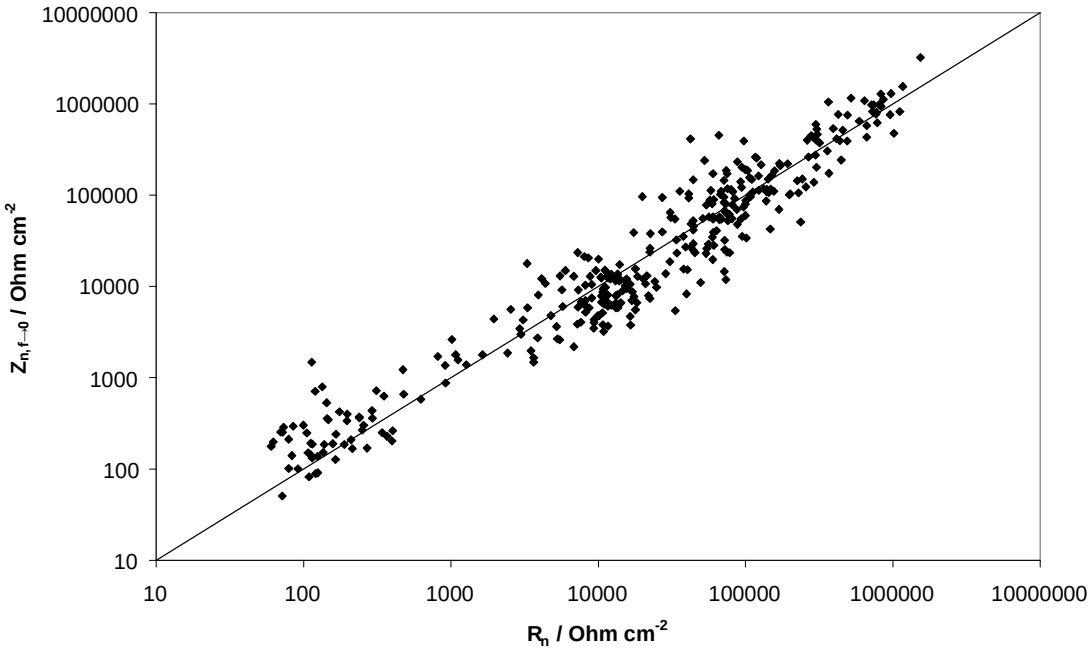

Figure 12 Comparison between R_n and $Z_{n,f\to0}$. Each point plotted corresponds to the data for a particular time record, while the solid line corresponds to $R_n = Z_{n,f\to0}$.